Figure S1. Detection of calcium phosphate particles in the lumen of proximal straight tubule by scanning electron microscopy (SEM) with energy dispersive X-ray spectroscopy (EDS). A semi-thin section stained with toluidine blue showing the junction of outer (OS) and inner (IS) stripes (**A**, **B**). The marked area (**A**) is magnified (**B**) in order to show multiple proximal tubules with brush borders (**B**, asterisks) in OS. The backscattered electron (BSE, inversed image) image of the marked area (**B**) in a serial section demonstrates tubular epithelium (Ep) with microvilli in the lumen (**C**, asterisk). The marked area in the proximal tubule (**C**) showing secondary electron (SE, **D**), BSE (**E**, inversed image) and EDS (**F-I**) images at higher magnification demonstrates small particles (**E**, arrowhead) with O (EDS-O, **F**, arrowhead), Ca (EDS-Ca, **G**, arrowhead) and P (EDS-P, **H**, arrowhead) signals but not Cl signal (EDS-Cl, **I**, arrowhead) observed in the lumen of the tubule surrounded by tubular epithelium (**E**, Ep) with microvilli (**E**, asterisks). At higher magnification of the marked area (**E**), the microvilli (**K**, asterisk) surround the particle (**J**, **K**, arrowheads) with O, Ca and P signals (**L**, **M**, **N**, arrowheads) but not Cl signal (**O**, arrowhead). Scale bars: 100 (**A,B**), 10 (**C-I**) or 5 (**J-O**) μm.
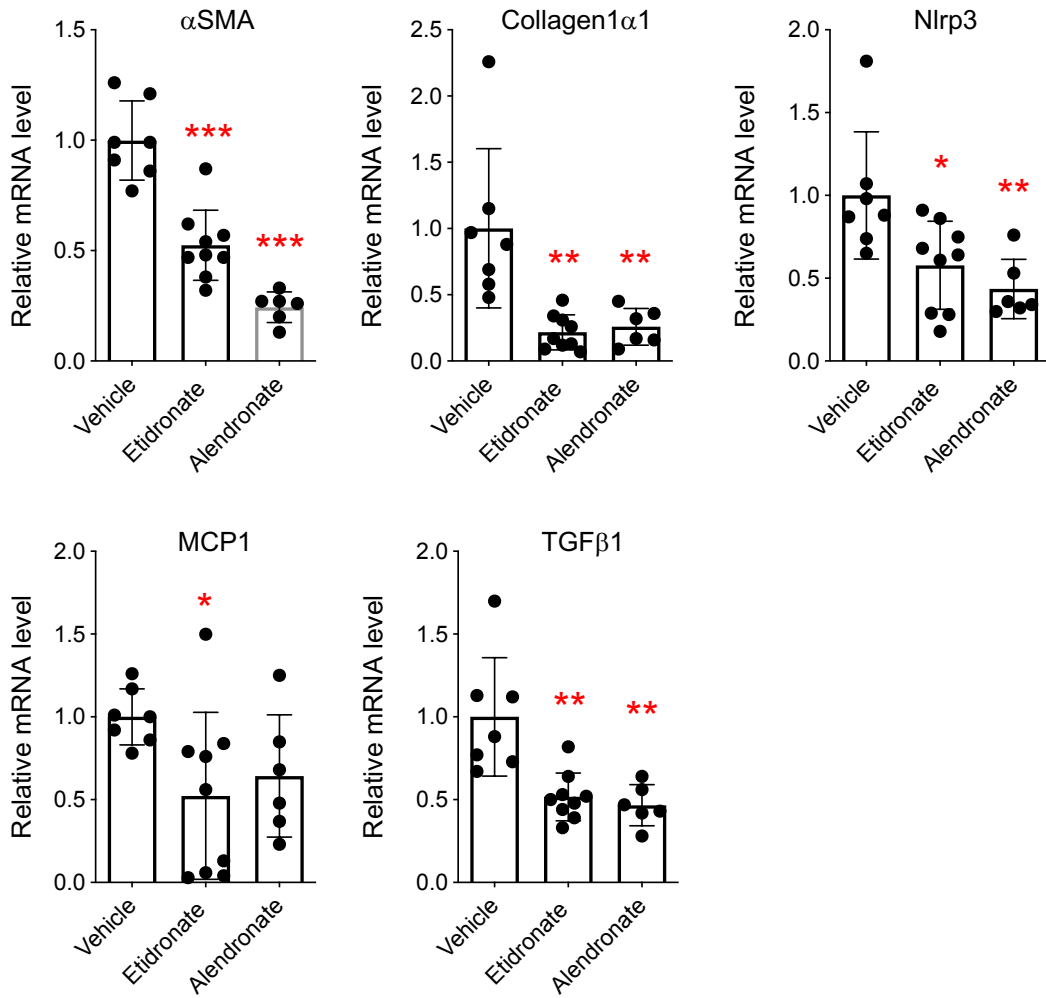
Figure S2. Effects of bisphosphonate on phosphate-induced renal fibrosis and inflammation. Mice (4-week-old C57BL/6 males) were placed on high phosphate diet containing 2.0% inorganic phosphate and subcutaneously injected with either etidronate (100 mg/kg, $N = 9$) or alendronate (10 mg/kg, $N = 6$) or vehicle (saline, $N = 7$) every other day for 8 weeks. Relative renal mRNA levels of α-smooth muscle actin (αSMA), collagen1α1, nucleotide-binding oligomerization domain-like receptor family pyrin domain-containing 3 (Nlrp3), monocyte chemotactic protein-1 (MCP1), and transforming growth factor-β1 (TGFβ1) were measured by quantitative RT-PCR (qPCR). The data were indicated as mean ± s.d. ***$P < 0.0001$, **$P < 0.01$, *$P < 0.05$ vs vehicle by 1-way ANOVA with Dunnett's multiple-comparison tests.
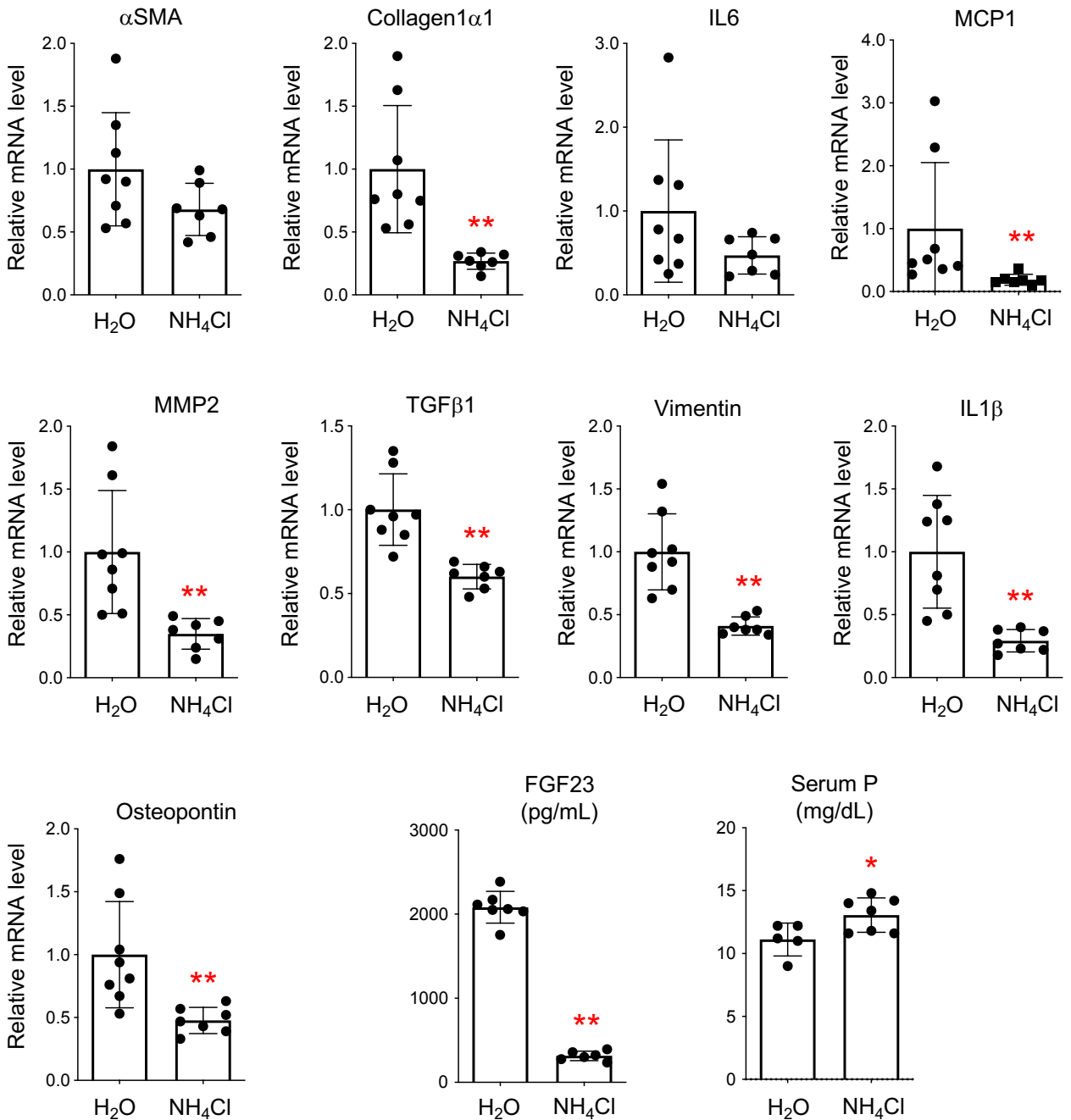
Figure S3. Effects of urine acidification on phosphate-induced renal fibrosis and inflammation. Mice (4-week-old C57BL/6 males) were placed on high phosphate diet containing 2.0% inorganic phosphate and given tap water (H_2O) or 0.14 M ammonium chloride solution (NH_4Cl) as drinking water for 8 weeks. Relative renal mRNA levels of α-smooth muscle actin (αSMA), collagen1α1, interleukin-6 (IL6), monocyte chemotactic protein-1 (MCP1), matrix metalloprotease-2 (MMP2), transforming growth factor-β1 (TGFβ1), vimentin, interleukin-1β (IL1β), and osteopontin were quantified by qPCR. Serum FGF23 and phosphate levels were measured as described in Methods. The data were indicated as mean ± s.d. *$P < 0.05$, **$P < 0.01$ vs H_2O by Mann-Whitney test, $N = 4$-8 for each group as indicated by dots.
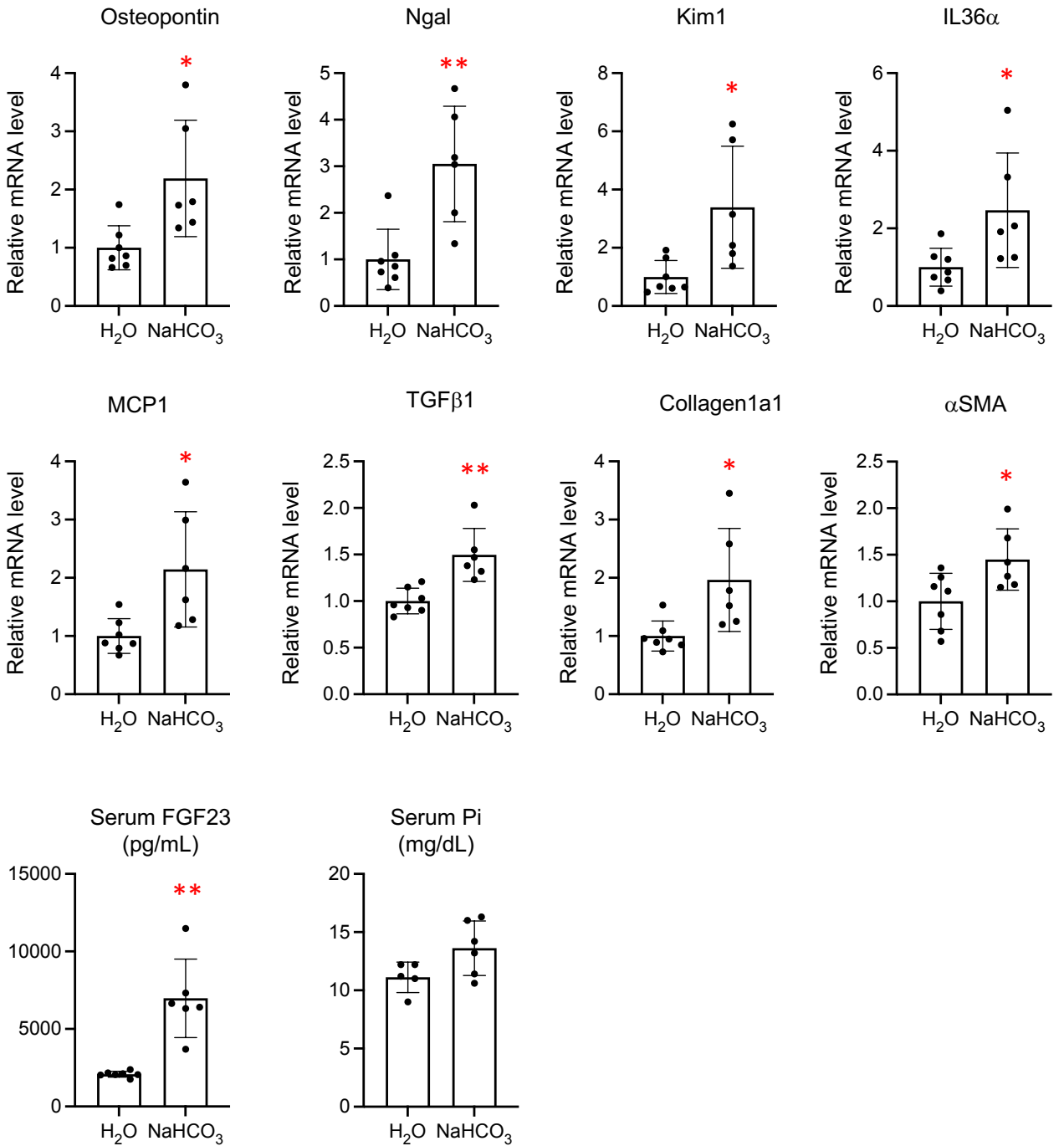
Figure S4. Effects of urine alkalization on phosphate-induced renal fibrosis and inflammation. Mice (12-week-old C57BL/6 males) were placed on high phosphate diet containing 2.0% inorganic phosphate and given tap water (H_2O) or 0.15 M sodium bicarbonate solution ($NaHCO_3$) as drinking water for 8 weeks. Relative renal mRNA levels of osteopontin, neutrophil gelatinase-associated lipocalin (Ngal), kidney injury molecule-1 (Kim1), interleukin-36α (IL36α), monocyte chemotactic protein-1 (MCP1), transforming growth factor-β1 (TGFβ1), collagen1α1, and α-smooth muscle actin (αSMA) were quantified by qPCR. Serum FGF23 and phosphate levels were measured as described in Methods. The data were indicated as mean ± s.d. *$P < 0.05$, **$P < 0.01$ vs H_2O by Mann-Whitney test, $N = 4$-8 for each group as indicated by dots.
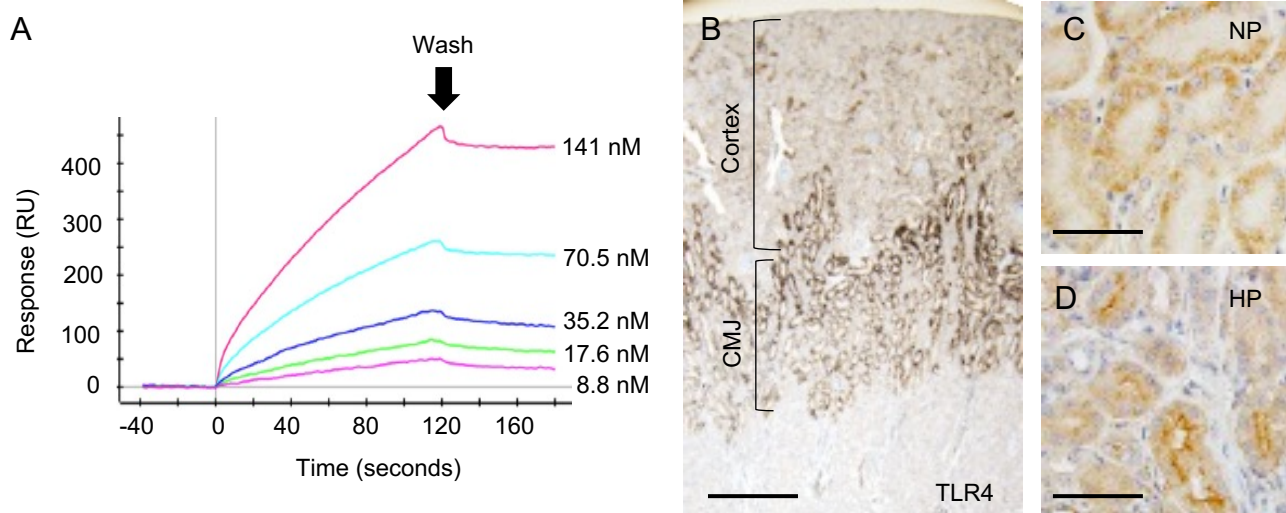
Figure S5. Calcium-phosphate particles bind to TLR4. (**A**) Physical interaction between calcium phosphate particles and TLR4 was evaluated by surface plasmon resonance. Recombinant TLR4 ectodomain protein was overlaid at the indicated concentrations over a sensor chip immobilized with calcium phosphate particles. The equilibrium dissociation constant ($K_D = 9.63 \times 10^{-9}$ M) was calculated from the association rate constant (ka $= 6.24 \times 10^4$ $M^{-1}s^{-1}$) and the dissociation rate constant (kd $= 6.01 \times 10^{-4}$ s^{-1}) determined by SPR. (**B**, **C**) Immunohistochemistry of kidney sections from mice fed the normal phosphate diet (0.35% phosphate) using an anti-TLR4 antibody. CMJ, cortico-medullary junction. (**D**) Accumulation of TLR4 on the apical membrane of the renal tubules in mice fed the high phosphate diet (2.0% phosphate, HP) . Bar = 200 μm in (**B**), Bar = 50 μm in (**C**, **D**).
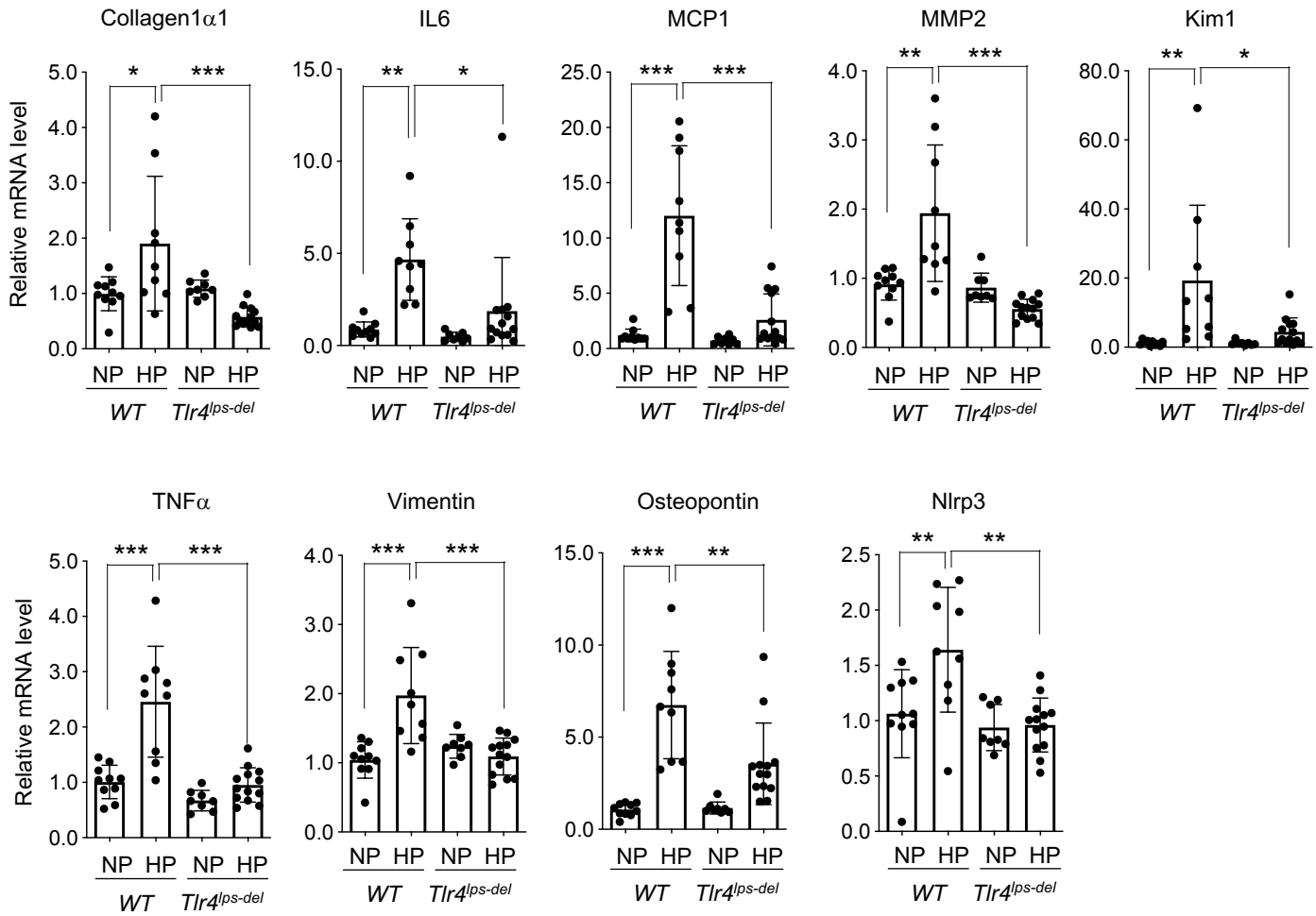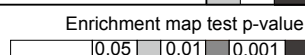
Figure S6. Mice lacking TLR4 are resistant to phosphate-induced renal tubular damage, inflammation, and fibrosis. Wild-type mice (4-week-old C57BL/6 males, *WT*) and *Tlr4*-deficient mice (4-week-old males, *Tlr4$^{lps-del}$*) were placed on either normal diet containing 0.35% inorganic phosphate (NP) or high phosphate diet containing 2.0% inorganic phosphate (HP) for 4 weeks. Relative renal mRNA levels of collagen1α1, interleukin-6 (IL6), monocyte chemotactic protein-1 (MCP1), matrix metalloprotease-2 (MMP2), kidney injury molecule-1 (Kim1), tumor necrosis factor-α (TNFα), vimentin, osteopontin, and nucleotide-binding oligomerization domain-like receptor family pyrin domain-containing 3 (Nlrp3) were measured by quantitative RT-PCR (qPCR). The data were indicated as mean ± s.d. N = 10, 8, 8, and 13 for *WT*;NP, *WT*;HP, *Tlr4$^{lps-del}$*;NP, *Tlr4$^{lps-del}$*;HP, respectively. *P < 0.05, **P < 0.01, ***P < 0.0001 1-way ANOVA with Tukey's multiple-comparison tests.

KEGG pathway	Time (h)		
	3	6	24
Oxidative phosphorylation			■
Glycerolipid metabolism			▥
Protein processing in endoplasmic reticulum			░
ABC transporters			░
Ras signaling pathway			■
Rap1 signaling pathway		■	■
MAPK signaling pathway			■
ErbB signaling pathway			■
Wint signaling pathway			▥
TGF-beta signaling pathway		▥	
Hippo signaling pathway			■
JAK-STAT signaling pathway			■
NF-kappa B signaling pathway			■
TNF signaling pathway			■
HIF-1 signaling pathway			■
Toll-like receptor signaling pathway		■	■
NOD-like receptor signaling pathway			■
RIG-I-like receptor signaling pathway			▥
T cell receptor signaling pathway			■
Fc epcilon RI signaling pathway			■
Chemokine signaling pathway			■
IL-17 signaling pathway	░	■	■
p53 signaling pathway			■
PPAR signaling pathway			■
Phospholipase D signaling pathway			░
Sphingolipid singnaling pathway			░
mTOR signaling pathway			░
FoxO signaling pathway			■
cAMP signaling pathway			■
PI3K-Akt signaling pathway			■
Cytokine-cytokine receptor interaction			■
Inlammatory mediator regulation of TRP channels			▥
Natural killer cell mediated cytotoxicity			■
Antigen processing and presentation			■
Th1 and Th2 cell differentiation			■
Th17 cell differentiation			▥
Fc gamma R-mediated phagocytosis			▥
Leukocyte transendothelial migration			■
Regulation of lipolysis in adipocytes			▥
Endocytosis			■
Autophagy			▥
ECM-recepotr interaction			■
Cell adhesion molecules (CAMs)			■
Focal adhesion			■
Tight junction			■
Gap junction	■	■	
Regulation of actin cytoskeleton			▥
Cell cycle			■
Apoptosis			■
Necrosis			■
Protein digestion and absorption			■
Mineral absorption			▥
Retrograde endocannabinoid signaling			■
Osteoclast differentiation		░	■

Enrichment map test p-value

| 0.05 | 0.01 | 0.001 | |

Figure S7. KEGG pathway analysis of HK-2 cells challenged with calcium phosphate particles. The pathways affected by calcium phosphate particles were identified by comparing between before and after incubation with synthesized calcium phosphate particles for 3, 6, or 24 hours, and shown as a heatmap.
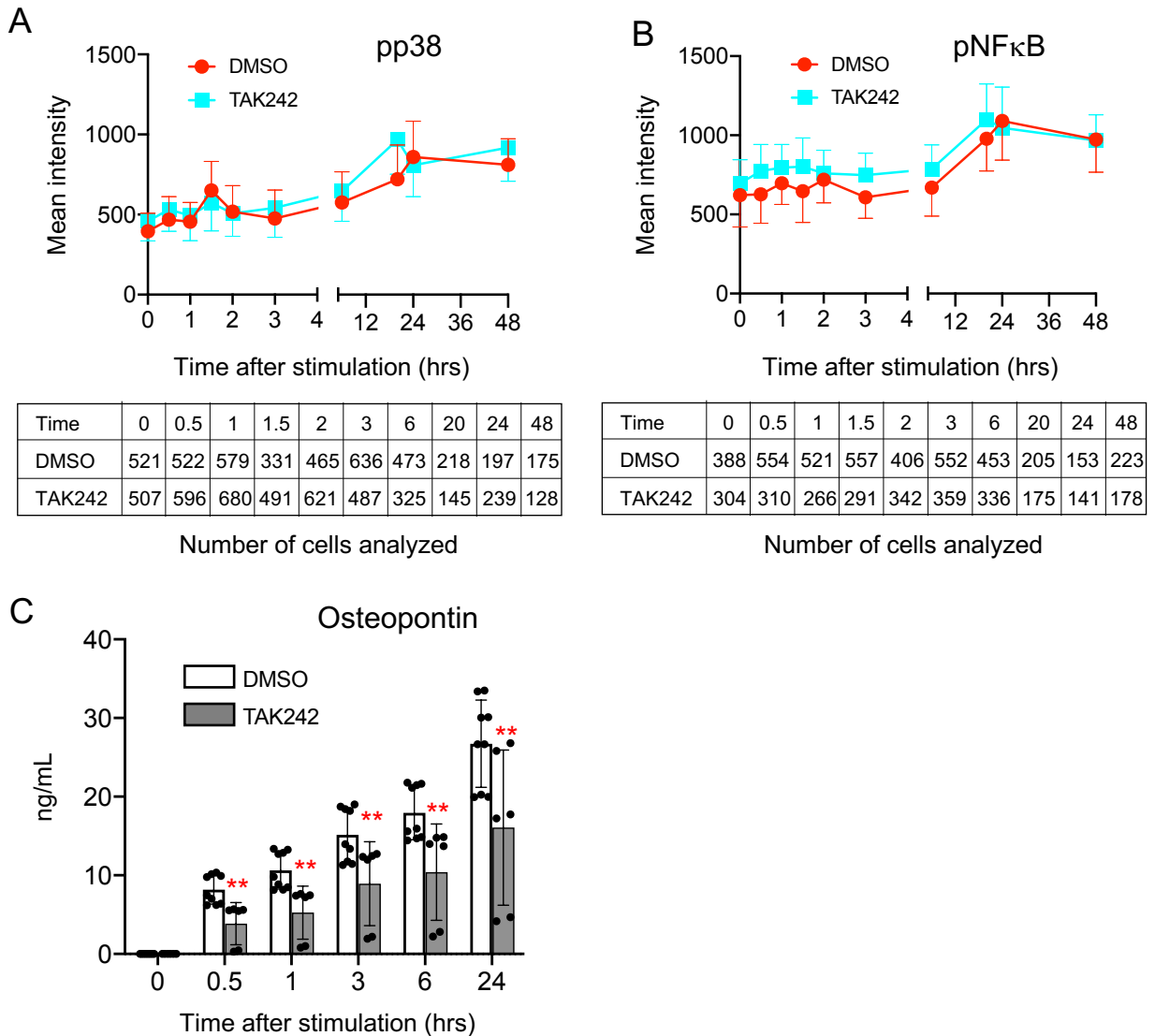
A

pp38

DMSO
TAK242

Mean intensity / Time after stimulation (hrs)

Time	0	0.5	1	1.5	2	3	6	20	24	48
DMSO	521	522	579	331	465	636	473	218	197	175
TAK242	507	596	680	491	621	487	325	145	239	128

Number of cells analyzed

B

pNFκB

DMSO
TAK242

Mean intensity / Time after stimulation (hrs)

Time	0	0.5	1	1.5	2	3	6	20	24	48
DMSO	388	554	521	557	406	552	453	205	153	223
TAK242	304	310	266	291	342	359	336	175	141	178

Number of cells analyzed

C

Osteopontin

DMSO
TAK242

ng/mL / Time after stimulation (hrs)

Figure S8. Relation between activation of TLR4 signaling and effects of calcium phosphate particles. HK-2 cells were incubated with synthesized calcium phosphate particles (10 μg phosphorus/mL) in the presence or absence of a cell-permeable inhibitor for TLR4 signaling activation (TAK242, 2 μM) for the indicated time periods. The HK-2 cells were subjected to immunocytochemical analysis using antibodies against phosphorylated p38 (**A**) and phosphorylated NFκB (**B**). Mean signal intensity from nuclei in the presence (TAK242, blue) or absence (DMSO, orange) of the inhibitor was measured as in **Fig. 4**. The data were indicated as mean ± s.d. N = number of cells analyzed for each time point. No significant difference was observed between DMSO and TAK242 in any time points. (**B**) Concentration of osteopontin was measured by ELISA in the conditioned medium of HK-2 cells incubated with calcium phosphate particles (10 μg phosphorus/mL) in the presence (TAK242, gray bars) or absence (DMSO, empty bars) of the inhibitor for the indicated time periods. N = 9 for DMSO, N = 6 for TAK242. **$P < 0.0001$ vs DMSO 2-way ANOVA with Šidák's multiple comparison test.
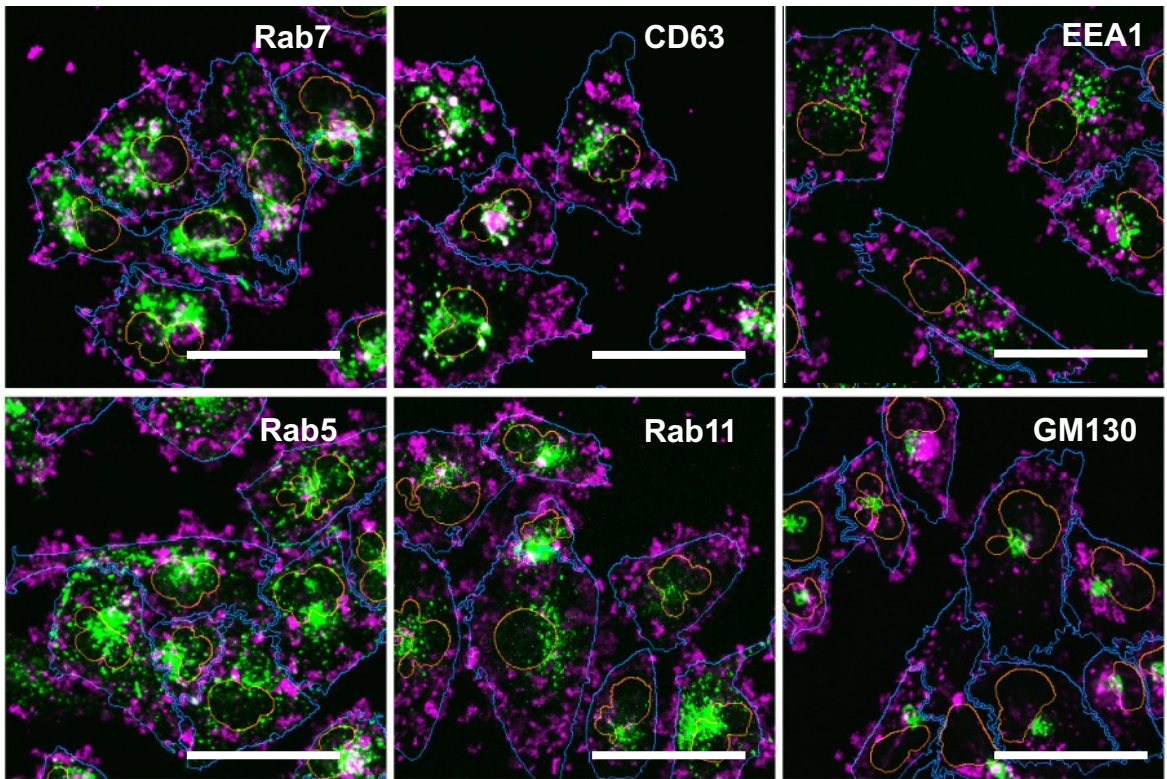
Figure S9. Effects of calcium phosphate particles on endosomal trafficking. HK-2 cells were incubated with synthesized calcium phosphate particles (10 μg phosphorus/mL) fluorescently labeled with 5(6)-RhR-dRIS for 24 hours and then subjected to immunocytochemistry using antibodies against Rab7 (late endosome), CD63 (lysosome), EEA1 (early endosome), Rab5 (early endosome), Rab11 (recycling endosome), and GM130 (Golgi). Typical confocal images are shown. Overlap between calcium-phosphate particles (magenta) and endosomal markers (green) appears white. Plasma membrane and nuclear membrane are depicted in blue and orange lines, respectively. Bar = 50 μm.
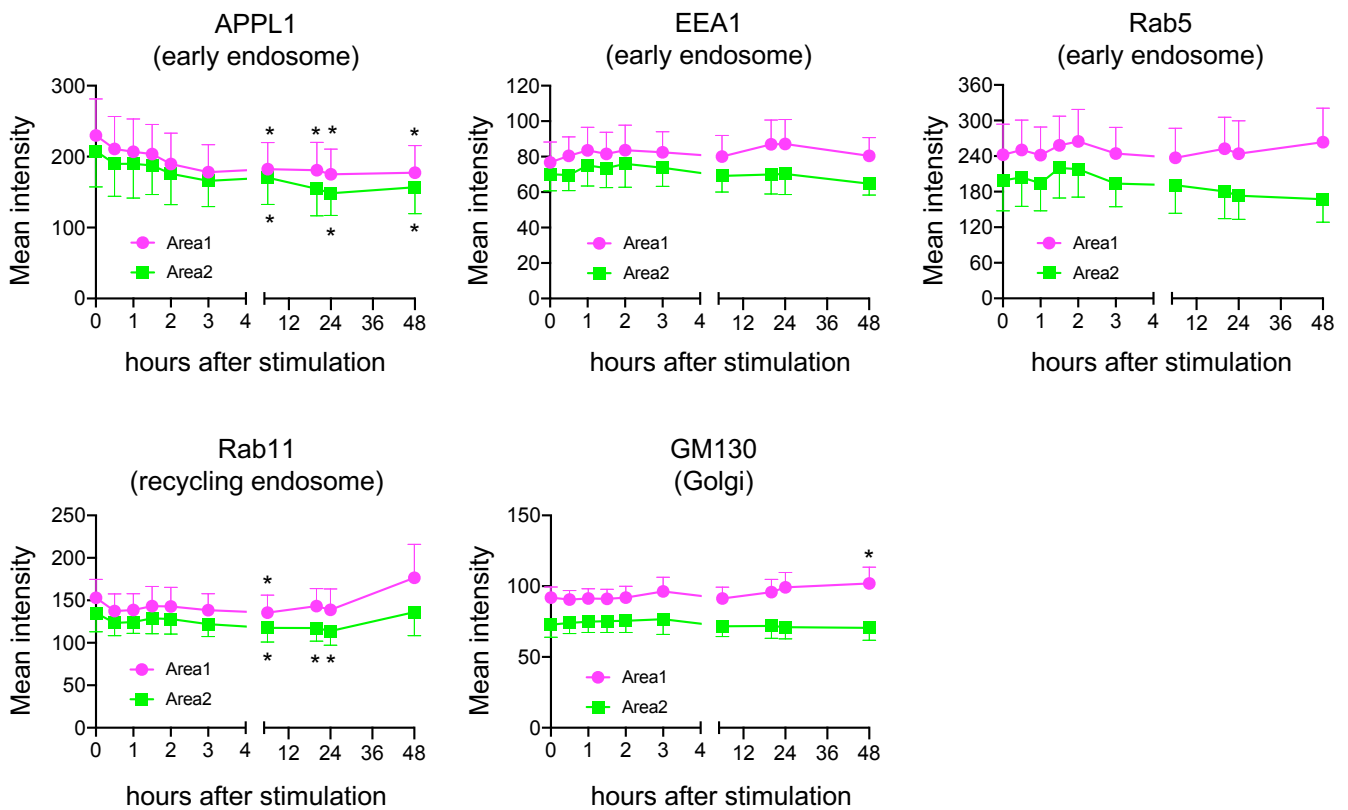
Figure S10. Effects of calcium phosphate particles on early endosomes, recycling endosomes, and Golgi. HK-2 cells were incubated with calcium-phosphate particles (10 μg phosphorus/mL) for indicated time periods and then subjected to immunocytochemistry using antibodies against APPL1, EEA1, Rab5, Rab11, and GM130. Confocal microscopic images were analyzed to determine the intensity of fluorescent signals in Area1 (perinuclear region, magenta) and Area2 (submembrane region, green). The data were indicated as mean ± s.d. N = number of cells analyzed for each time point. *Effect size > 0.5 vs time 0 (before stimulation with calcium phosphate particles) by Brunner-Munzel test.
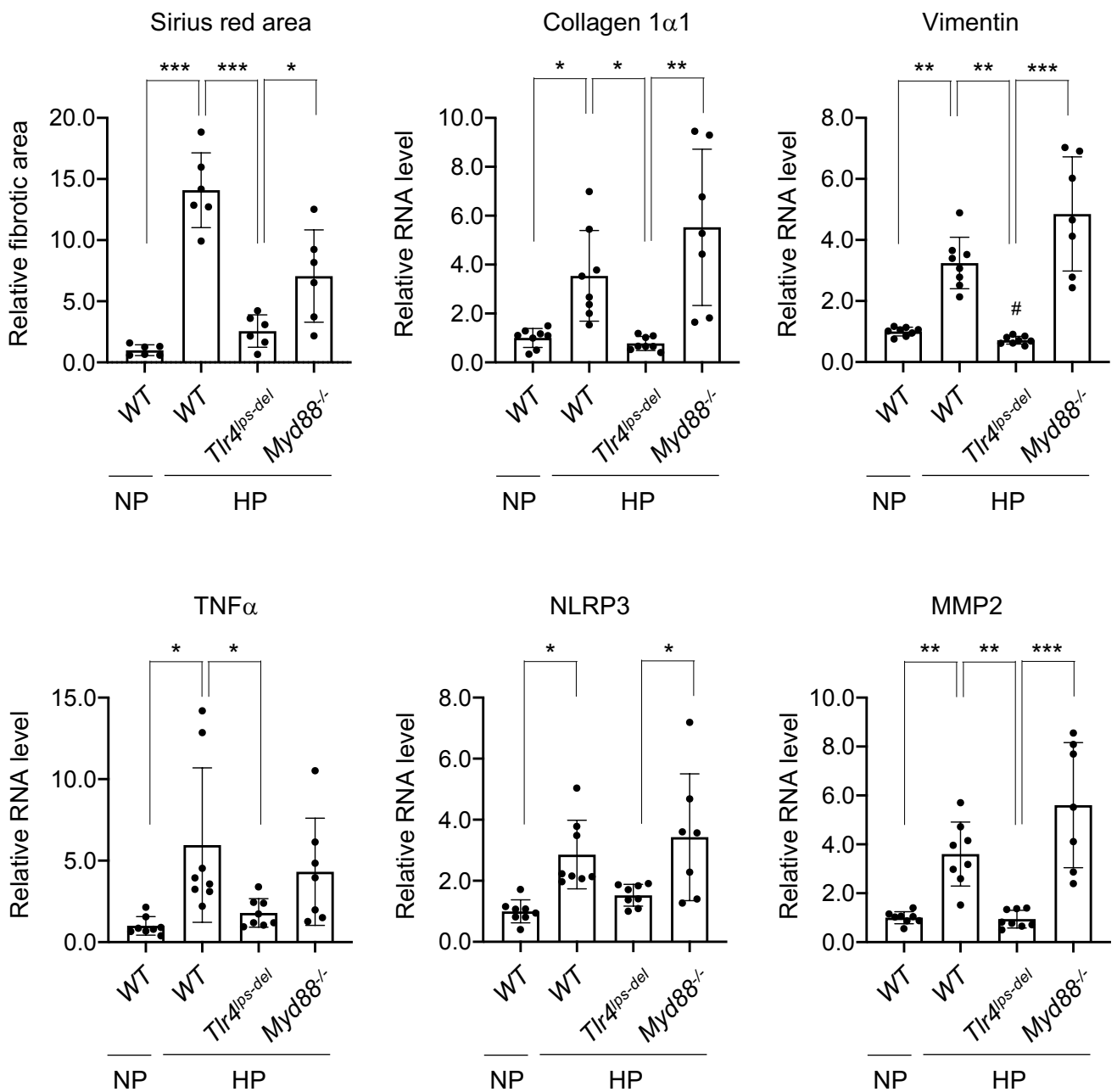
Figure S11. Mice lacking TLR4, but not MyD88, are resistant to phosphate-induced renal fibrosis. Wild-type mice (4-week-old C57BL/6 males, *WT*), TLR4 deficient mice (4-week-old *Tlr4$^{lps-del}$* males), and MyD88 deficient mice (4-week-old *MyD88$^{-/-}$* males) were placed on normal diet containing 0.35% inorganic phosphate (NP) or high phosphate diet containing 2.0% inorganic phosphate (HP) for 4 weeks. Relative fibrotic areas of the kidneys were detected by Sirius-red staining of regular paraffin sections and quantified. Relative renal mRNA levels of collagen1α1, vimentin, tumor necrosis factor-α (TNFα), nucleotide-binding oligomerization domain-like receptor family, pyrin domain-containing 3 (Nlrp3), and matrix metalloprotease-2 (MMP2) were measured by quantitative RT-PCR (qPCR). The data were indicated as mean ± s.d. $N = 8$, 8, 8, and 7 for *WT*;NP, *WT*;HP, *Tlr4$^{lps-del}$*;HP, *MyD8$^{-/-}$*;HP, respectively. *$P < 0.05$, **$P < 0.01$, ***$P < 0.0001$ by 1-way ANOVA with Tukey's multiple-comparison tests.

A
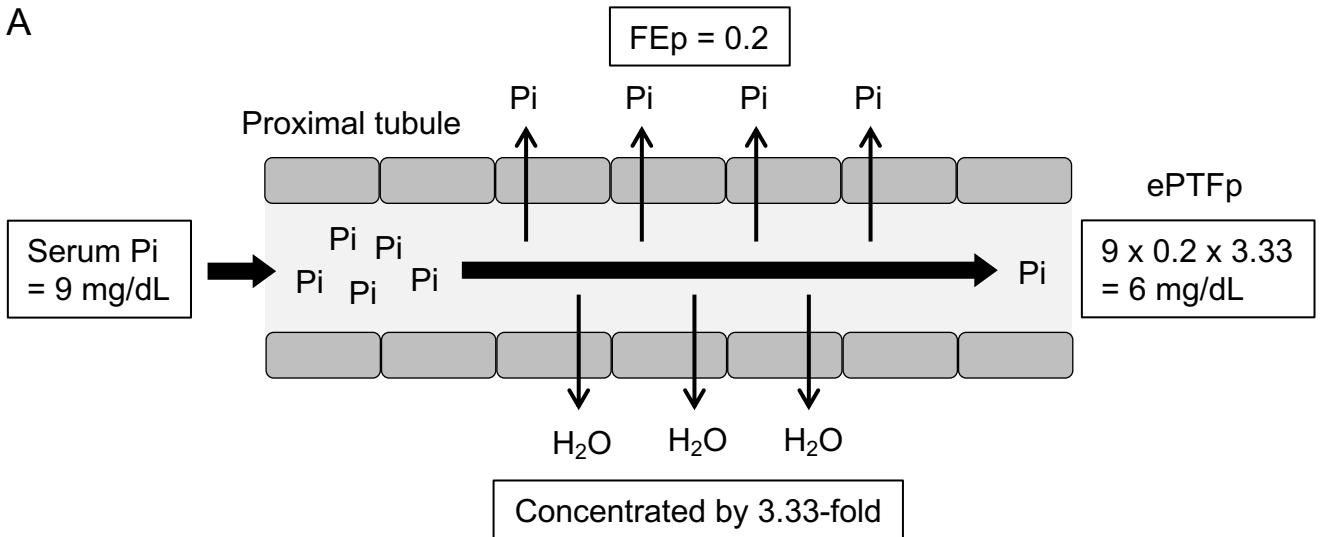
	Sp (mg/dl)	FEp	actual PTFp (mg/dl)	ePTFp (mg/dl)
Group I: Control	7.6	0.1	2.3	2.5
Group II: Phosphate load	18.4	0.4	29.4	24.5
Group III: Subtotal nephrectomy	7.3	0.6	11.7	14.6

Figure S12. Estimated phosphate concentration in the proximal tubular fluid (ePTFp). (A) An example for calculation of ePTFp. Assuming that the serum phosphate level is 9 mg/dL and that the fractional excretion of phosphate (FEp) is 0.2, phosphate concentration in the tubular fluid at the distal portion of proximal tubules is estimated as 6 mg/dL. (**B**) Bank *et al*. directly measured phosphate concentration of the renal tubular fluid by micropuncture in living SD rats[20]. Three groups of rats were set up; Group I: control rats (normal SD rats), Group II: phosphate-loaded rats (intravenous infusion of 0.3M sodium phosphate at the speed of 2.3 ml/h), Group III: subtotal-nephrectomized rats. In the Bank's paper, available data included the average of plasma phosphate (Sp), fractional excretion of phosphate (FEp), and the ratio of phosphate concentration in the tubular fluid to that in the plasma (TF/P). Based on these data, estimated PTFp (ePTFp) calculated from Sp and FEp was compared with the actual PTFp in each group. The actual PTFp was similar to ePTFp.